Dispersion inversion of electromagnetic pulse propagation within freezing and thawing soil waveguides

J. van der Kruk,[1,2] C. M. Steelman,[3] A. L. Endres,[3] and H. Vereecken[1]

Received 16 June 2009; revised 23 July 2009; accepted 14 August 2009; published 24 September 2009.

[1] Freeze and thaw processes are important components in characterizing glacial, periglacial and frozen ground environments, and hence the response of cryospheric regions to climate change. High-frequency ground-penetrating radar is particularly well suited for monitoring the freezing and thawing processes within the shallow subsurface (i.e., < 1 m depth) due to its non-invasive nature and its sensitivity to the liquid water component in soil. The freezing of moist soil and thawing of frozen soil induce leaky and low-velocity waveguides, respectively. Within these waveguide layers, the internally reflected radar energy produces interfering multiples that appear as a package of dispersed waves. Here, we present a new method for characterizing very shallow freeze and thaw processes, in which the waveguide properties are obtained by inverting the observed dispersion curves. This new method can non-invasively monitor freezing and thawing processes in a wide range of glacial, periglacial and frozen ground studies. **Citation:** van der Kruk, J., C. M. Steelman, A. L. Endres, and H. Vereecken (2009), Dispersion inversion of electromagnetic pulse propagation within freezing and thawing soil waveguides, *Geophys. Res. Lett.*, *36*, L18503, doi:10.1029/2009GL039581.

1. Introduction

[2] The freezing and thawing of near-surface material are important processes in cryospheric environments. The depth and distribution of frozen zones not only influence the dynamics of soil water distribution, but also have significant implications for modelling a wide-range of atmospheric and subsurface processes. We propose that high frequency (> 250 MHz) ground-penetrating radar (GPR) is particularly well suited for monitoring the freezing and thawing process within the shallow subsurface because of its non-invasive nature and ability to obtain a measure of the liquid water component in frozen soil.

[3] GPR is often used to characterize glacial and permafrost environments [*Woodward and Burke*, 2007; *Kneisel et al.*, 2008]. While numerous studies have successfully used GPR to evaluate the spatial and temporal distribution of ground ice, depth to permafrost table and thickness of the active layer above the permafrost [e.g., *Annan and Davis*, 1978; *Delany et al.*, 1990; *Arcone et al.*, 1998; *Hinkel et al.*, 2001; *Moorman et al.*, 2003; *De Pascale et al.*, 2008], only recently has high-frequency GPR been used to monitor seasonal frost development in mid-latitude climates [*Steelman and Endres*, 2009].

[4] The permittivity of ice and water are approximately $3\varepsilon_0$ and $80\varepsilon_0$, respectively, where ε_0 is the permittivity of free space. Due to this large contrast, the permittivity of wet soils can change dramatically during the freezing and thawing process. *Arcone et al.* [1998] found that the dielectric permittivity decreased by a factor of 4 or more at the saturated sediment-permafrost boundary. Due to this strong contrast in electromagnetic properties, *Moorman et al.* [2003] was able to use GPR to image periglacial conditions, while *Bradford et al.* [2005] successfully measured the thaw depth beneath peat-lined arctic streams.

[5] When the thickness of the frozen sand overlying wet thawed sand or the thawed layer overlying the frozen sand is comparable to or smaller than the in situ wavelength of the electromagnetic (EM) waves emitted by the GPR system, the frozen or thawed sand layer act as a waveguide in which the EM energy is internally reflected. This results in a series of interfering multiples that manifest themselves as a package of dispersed waves which propagate large distances at phase and group velocities that may not correspond to material dielectric properties. These dispersed EM waves contain important information about the nature of the waveguide. However, standard travel-time techniques for estimating the velocity and thickness of the waveguide from a common-midpoint (CMP) measurement cannot be applied, because the different phases cannot be clearly identified.

[6] The unfrozen soil underlying the shallow frozen layer will generate a strong reflection because it has a much higher relative permittivity. Total internal reflection only occurs at the upper interface beyond the critical angle. While the lower interface is a strong reflector, some energy is still transmitted across the interface; hence, it is a leaky waveguide (Figure 1a). For the thawed layer case, the underlying frozen soil layer has a relatively lower permittivity, giving rise to a critical refraction. Here, the thawed layer has the lowest velocity and is called the low-velocity waveguide. Total internal reflection occurs at both interfaces when the angle of incidence is larger than the critical angle of the lower interface (Figure 1b). The freezing and thawing cycle in mid-latitude climates results in the presence of a leaky and a low-velocity waveguide at the same location over time.

[7] For the leaky waveguide, *Arcone* [1984] investigated the electromagnetic properties of ice sheets overlying water. Given the average thickness of the waveguide, he determined the dielectric permittivities of the ice layer by assuming that the dominant frequencies of the dispersive coupled air-ice waves were accurate predictions of the waveguide cutoff frequencies. Recently, the derivation of

[1]Forschungszentrum Juelich GmbH, ICG4 Agrosphere, Juelich, Germany.
[2]Formerly at ETH Zurich, Zurich, Switzerland.
[3]Department of Earth and Environmental Sciences, University of Waterloo, Waterloo, Ontario, Canada.

0094-8276/09/2009GL039581

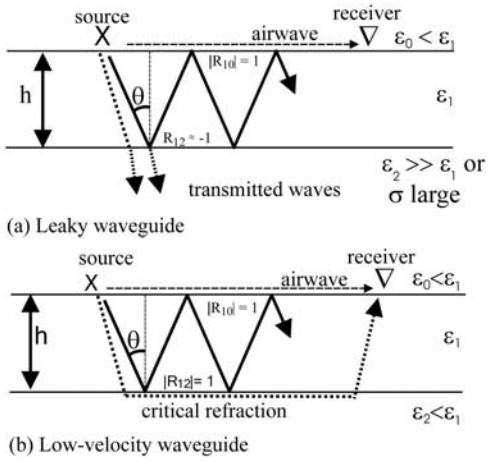

Figure 1. Diagram of the (a) leaky and (b) low-velocity waveguides. Arrows show dominant ray paths of the EM waves.

dispersion curves from GPR data measured across ice sheets overlying water and their subsequent inversion have been described by *van der Kruk et al.* [2007]. Procedures for inverting dispersion curves, which are analogous to techniques recently developed for analyzing surface waves recorded on multichannel seismic data, were derived for transverse-electric (TE) and transverse-magnetic (TM) GPR data. *Liu and Arcone* [2003] showed with finite-difference time-domain modeling that the TE mode emits more energy in the ground than the TM mode.

[8] For the low-velocity waveguide, *Arcone et al.* [2003] studied the characteristics of EM waves traveling through a thin surface waveguide of low-velocity (high-permittivity) wet soil underlain by high-velocity (low-permittivity) dry sand and gravel. Given the average thickness of the waveguide, they were able to derive the relative permittivities of the two layers from the highly dispersed waveforms. Recently, the derivation of dispersion curves from GPR data and their subsequent inversion for subsurface-medium properties have been described by *van der Kruk et al.* [2006]. Using these procedures, accurate model parameters were derived from synthetic and field data. To obtain meaningful models from GPR data characterized by discontinuous dispersed phases, a joint inversion of the TE and TM field data was necessary [*van der Kruk et al.*, 2006]. Including higher order modes in the inversion resulted in more accurate predictions of material physical properties [*van der Kruk*, 2006].

[9] In this paper, we show that both the leaky and low-velocity waveguides are induced by freezing moist sand and by thawing frozen sand, respectively. In both cases, the waveguide properties can be obtained by calculating phase-velocity spectra, followed by determining the dispersion curves from the maxima in the spectra. We then invert the observed curves using a procedure based on single-layer subsurface models to obtain the physical properties of the thawed and frozen soils.

2. Dispersion Inversion

[10] Dispersion is a typical feature of seismological data at all scales: Dispersed Rayleigh waves are commonly used to infer subsurface material properties. In shallow seismological studies, the dispersed Rayleigh waves recorded on multichannel data are first transformed from the time-distance domain to the phase-velocity-frequency domain from which the optimum phase velocity versus frequency curve is determined. The derived dispersion curve is then inverted to obtain a layered subsurface model, which requires adjusting the model parameters until the difference between the observed dispersion curve and the theoretical dispersion curve for the model is minimized. In this way, shear-wave velocities [*Xia et al.*, 1999; *Park et al.*, 1999] can be determined. Recently, similar inversion techniques were applied to dispersive GPR data [*van der Kruk*, 2006; *van der Kruk et al.*, 2006, 2007].

[11] Here, we employ the method of *Park et al.* [1999] to calculate phase-velocity spectra of our GPR common midpoint (CMP) data. By selecting the maxima in the phase-velocity spectra, we obtain dispersion curves that show phase velocity as a function of frequency. The medium properties are obtained by inverting these dispersion curves. Due to the strong nonlinear nature of the forward problem, we employ a combined global and local optimization algorithm. For a variety of starting models, we initiated a local minimization algorithm based on the simplex search method [*Lagarias et al.*, 1998]. For each starting model, a local minimum is obtained. The local minimum that produces the closest match between the model and observed dispersion curves is regarded as the global minimum. To avoid the possibility of obtaining a very low cost function when only a few frequencies are used in the inversion, we required that the theoretical dispersion curve match the observed dispersion curve over at least 90% of the frequency range. Because we approximate the reflection coefficient between the waveguide and the lower halfspace at -1 for the leaky waveguide, the inversion depends on ε_1 and h [*van der Kruk et al.*, 2007], whereas the inversion for the low-velocity waveguide depends on ε_1, ε_2 and h [*van der Kruk et al.*, 2006].

3. Experimental Procedures

[12] Common-midpoint gathers were collected during the 2007 and 2008 winter seasons at a test site near Waterloo, Ontario, Canada, using a Sensors and Software PulseEKKO 1000 GPR system (Sensors and Software Inc., Mississauga, ON, Canada) equipped with 900 MHz bistatic antennas. The GPR data were acquired with a spatial and temporal sampling of 0.02 m and 0.1 ns, respectively. Surveys were conducted during the development of a seasonal frost layer and a period of seasonal thaw at a single measurement location characterized by well-sorted sandy soil. Since the freezing and thawing processes took place at very shallow depths, we used 900 MHz bistatic antennas. For larger depths, lower frequency antennas should be used.

3.1. Leaky Waveguide

[13] Figure 2a shows the GPR data measured across the leaky waveguide case of frozen sand overlying wet sand. Although many multiple reflections are apparent, it is not possible to uniquely identify each one. In contrast, the corresponding phase-velocity spectrum in Figure 2b clearly shows the presence of 4 TE modes. The maximum amplitude is normalized to unity for each frequency. The picked

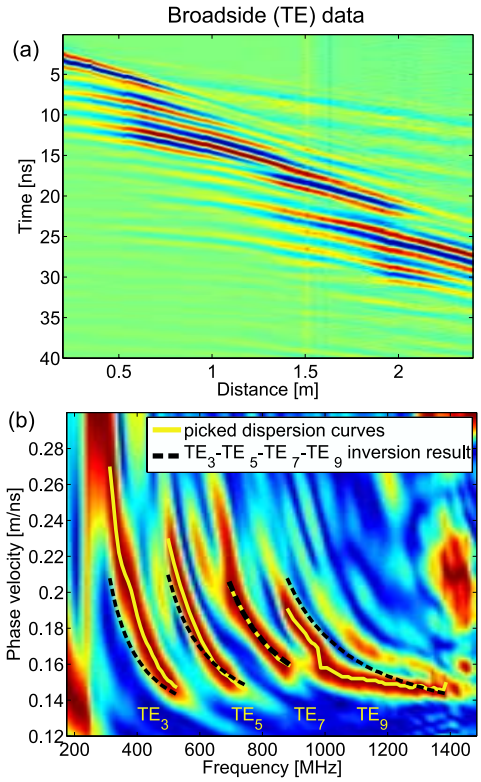

Figure 2. (a) Measured broadside leaky waveguide data set clearly showing the many multiples traveling within the frozen ground layer. (b) Corresponding phase-velocity spectrum. The yellow lines are the observed dispersion curves used for the inversion. The dashed black lines show the dispersion curves for the model obtained from the TE_3-TE_5-TE_7-TE_9 inversion result.

dispersion curves (yellow lines in Figure 2b) describe the loci of maximum amplitudes and hence are the solutions for the phase velocities. The high phase-velocity values close to that of air indicate a leaky waveguide, because leaky-waveguide dispersion curves always have values between that of air and the material within the waveguide [*van der Kruk et al.*, 2007]. After analyzing the frequency separation between the dispersion curves and using the formula for the cut-off frequency [*van der Kruk et al.*, 2007], we identified these phases as the TE_3, TE_5, TE_7, and TE_9 modes. Combining higher order modes better constrains the inversion in comparison to the separate inversion of each mode [*van der Kruk*, 2006]. Therefore, we performed a joint TE_3-TE_5-TE_7-TE_9 inversion of the observed dispersion curves shown in Figures 2a and 2b. For each suite of inversions, we used 9 different starting models with all combinations of ε_1 = 4, 12, and 20 and h = 0.05, 0.175, and 0.3 m. The optimal model parameters for the TE_3-TE_5-TE_7-TE_9 inversion are $\varepsilon_1 = 6.1$ and $h = 0.40$ m. Several local minima had these or similar values indicating that this inversion is well constrained. The black dashed lines in Figure 2b show the model dispersion curves obtained from the TE_3-TE_5-TE_7-TE_9 inversion, which fit the four modes reasonably well, with slightly larger deviations at lower and higher frequencies. Because the effective frequency spectrum had a maximum around 800 MHz, the fit of the TE_7 mode is judged to be more important than the fit of the TE_3, TE_5 and TE_9 modes.

3.2. Low-Velocity Waveguide

[14] Figures 3a and 3b show the broadside (TE) and endfire (TM) data, respectively, measured over thawing of the shallow part of the frozen ground. Both data sets clearly show shingling, which indicates significant dispersion. This

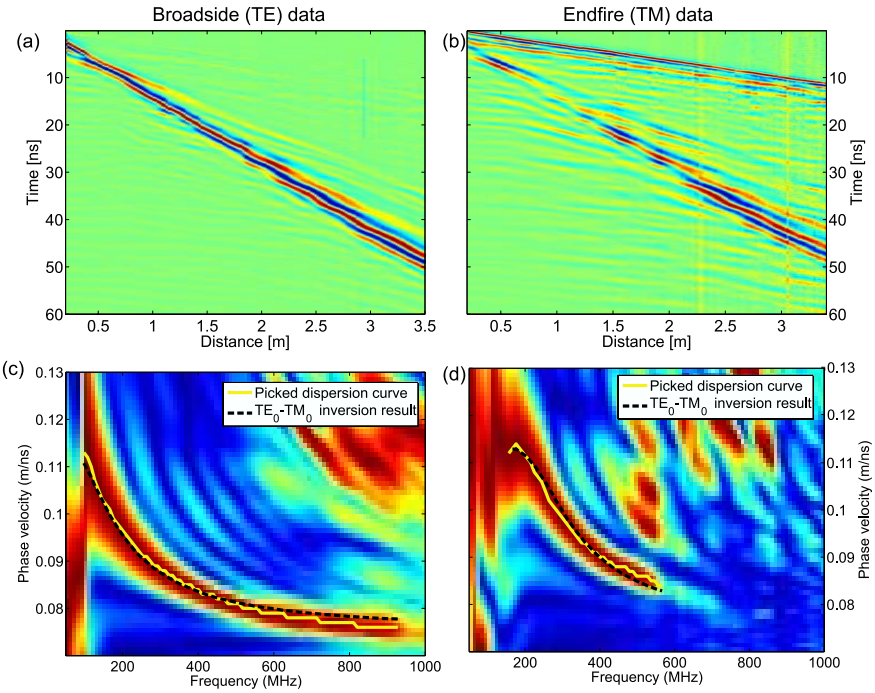

Figure 3. Measured (a) broadside and (b) endfire low-velocity waveguide data sets clearly showing dispersion, and (c and d) corresponding phase-velocity spectra, respectively. The yellow line is the observed dispersion curve used for the inversion. The dashed black lines represent the dispersion curve for the model obtained from the TE_0-TM_0 inversion result.

dispersion is more evident in the corresponding phase-velocity spectra (Figures 3c and 3d). Here, we could only identify the fundamental modes, which we obtained by picking the maxima in the phase-velocity spectra. Since joint inversions of the complementary TE and TM data provide results that are more reliable than those provided by the separate TE or TM inversions [*van der Kruk et al.*, 2006], we performed a joint TE_0-TM_0 inversion of the observed dispersion curves (yellow lines displayed in Figures 3c and 3d). Different local minima were obtained for 27 starting models (all combinations of $\varepsilon_1 = 10$, 15, and 20, $\varepsilon_2 = 3$, 6, and 9 and $h = 0.05$, 0.25 and 0.5 m). The optimal value of model parameters for the TE_0-TM_0 inversion are $\varepsilon_1 = 15.7$, $\varepsilon_2 = 7.0$ and $h = 0.15$ m. Again, several local minima had these or similar medium properties, indicating that this inversion is well constrained. We have plotted the computed TE_0 and TM_0 dispersion curves for the models on the TE and TM phase-velocity spectra of Figures 3c and 3d (black dashed lines). They show a reasonably good fit with the observed dispersion curves.

4. Conclusions

[15] Both the leaky and low-velocity waveguides are induced by seasonally frozen sand overlying wet sand and thawed sand overlying frozen sand, respectively. In both cases, the waveguide properties (layer dielectric permittivity and thickness) can be obtained by calculating phase-velocity spectra, followed by determining dispersion curves. For the leaky waveguide of frozen sand overlying wet sand, we identified and used 4 higher-order TE modes to invert for waveguide properties. The low-velocity waveguide, caused by thawing of the shallow part of the frozen soil, showed clear dispersion of the fundamental TE and TM modes; a joint inversion was used to obtain the waveguide properties. Here, we used 900 MHz antennas to investigate the freezing and thawing processes at very shallow depths. Larger depths can be investigated as long as the waveguide thickness is comparable to the in situ wavelength. This new method of characterizing near-surface freeze and thaw processes can be extended to a wide-range of glacial, periglacial and frozen ground studies, thereby improving our ability to monitor the effects of climate change in these sensitive environments.

[16] **Acknowledgments.** This work was partly supported by a grant from ETH Zurich and by an Individual Discovery Grant to A. L. Endres and a Post Graduate Scholarship (PGS-M and PGS-D) to Colby Steelman from the Natural Science and Engineering Research Council of Canada. We also thank Alicia and Murray Smith for the use of their property as our test site.

References

Annan, A. P., and J. L. Davis (1978), High frequency electrical methods for the detection of freeze-thaw interfaces, in *Proceedings of the Third International Conference on Permafrost*, pp. 495–500, Natl. Res. Counc. of Can., Ottawa, Ont., Canada.

Arcone, S. A. (1984), Field observations of electromagnetic pulse propagation in dielectric slabs, *Geophysics*, *40*, 285–298.

Arcone, S. A., D. E. Lawson, A. J. Delaney, and J. D. Strasser (1998), Ground-penetrating radar reflection profiling of groundwater and bedrock in an area of discontinuous permafrost, *Geophysics*, *63*, 1573–1584.

Arcone, S. A., P. R. Peapples, and L. Liu (2003), Propagation of a ground-penetrating radar (GPR) pulse in a thin-surface waveguide, *Geophysics*, *68*, 1922–1933.

Bradford, J. H., J. P. McNamara, W. Bowden, and M. N. Gooseff (2005), Measuring thaw depth beneath peat-lined arctic streams using ground-penetrating radar, *Hydrol. Processes*, *19*, 2689–2699.

Delaney, A. J., S. A. Arcone, and E. F. Chacho Jr. (1990), Winter short-pulse studies on the Tanana River, Alaska, *Arctic*, *43*, 244–250.

De Pascale, G. P., W. H. Pollard, and K. K. Williams (2008), Geophysical mapping of ground ice using a combination of capacitive coupled resistivity and ground-penetrating radar, Northwest Territories, Canada, *J. Geophys. Res.*, *113*, F02S90, doi:10.1029/2006JF000585.

Hinkel, K. M., J. A. Doolittle, J. G. Bockheim, F. E. Nelson, R. Paetzold, J. M. Kimble, and R. Travis (2001), Detection of subsurface permafrost features with ground-penetrating radar, Barrow, Alaska, *Permafrost Periglacial Processes*, *12*, 179–190.

Kneisel, C., C. Hauck, R. Fortier, and B. Moorman (2008), Advances in geophysical methods for permafrost investigations, *Permafrost Periglacial Processes*, *19*, 157–178.

Lagarias, J. C., J. A. Reeds, M. H. Wright, and P. E. Wright (1998), Convergence properties of the Nelder-Mead simplex method in low dimensions, *Soc. Ind. Appl. Math.*, *9*, 800–808.

Liu, L., and S. A. Arcone (2003), Numerical simulation of the wave-guide effect of the near-surface thin layer on radar wave propagation, *J. Environ. Eng. Geophys.*, *8*, 133–141.

Moorman, B. J., S. D. Robinson, and M. M. Burgess (2003), Imaging periglacial conditions with ground-penetrating radar, *Permafrost Periglacial Processes*, *14*, 319–329.

Park, C. B., R. D. Miller, and J. Xia (1999), Multichannel analysis of surface waves, *Geophysics*, *64*, 800–808.

Steelman, C., and A. L. Endres (2009), Evolution of high-frequency ground-penetrating radar direct ground wave propagation during thin frozen soil layer development, *Cold Reg. Sci. Technol.*, *57*, 116–122.

van der Kruk, J. (2006), Properties of surface waveguides derived from inversion of fundamental and higher mode dispersive GPR data, *IEEE Trans. Geosci. Remote Sens.*, *44*, 2908–2915.

van der Kruk, J., R. Streich, and A. G. Green (2006), Properties of surface waveguides derived from separate and joint inversion of dispersive TE and TM GPR data, *Geophysics*, *71*, K19–K29.

van der Kruk, J., S. A. Arcone, and L. Liu (2007), Fundamental and higher mode inversion of dispersed GPR waves propagating in an ice layer, *IEEE Trans. Geosci. Remote Sens.*, *45*, 2483–2491.

Woodward, J., and M. J. Burke (2007), Applications of ground-penetrating radar to glacial and frozen materials, *J. Environ. Eng. Geophys.*, *12*, 69–85.

Xia, J., R. D. Miller, and C. B. Park (1999), Estimation of near-surface shear-wave velocity by inversion of Rayleigh waves, *Geophysics*, *64*, 691–700.

A. L. Endres and C. M. Steelman, Department of Earth and Environmental Sciences, University of Waterloo, Waterloo, ON N2L 3G1, Canada.

J. van der Kruk and H. Vereecken, Forschungszentrum Juelich GmbH, ICG4 Agrosphere, Leo-Brandt-strasse, D-52425 Juelich, Germany. (j.van.der.kruk@fz-juelich.de)